Combined valence bond-molecular mechanics potential-energy surface and direct dynamics study of rate constants and kinetic isotope effects for the $H+C_2H_6$ reaction

Arindam Chakraborty, Yan Zhao, Hai Lin,[a] and Donald G. Truhlar[b]
Department of Chemistry and Supercomputing Institute, University of Minnesota, Minneapolis, Minnesota 55455-0431

(Received 18 August 2005; accepted 11 October 2005; published online 27 January 2006)

This article presents a multifaceted study of the reaction $H+C_2H_6 \rightarrow H_2+C_2H_5$ and three of its deuterium-substituted isotopologs. First we present high-level electronic structure calculations by the W1, G3SX, MCG3-MPWB, CBS-APNO, and MC-QCISD/3 methods that lead to a best estimate of the barrier height of 11.8 ± 0.5 kcal/mol. Then we obtain a specific reaction parameter for the MPW density functional in order that it reproduces the best estimate of the barrier height; this yields the MPW54 functional. The MPW54 functional, as well as the MPW60 functional that was previously parametrized for the $H+CH_4$ reaction, is used with canonical variational theory with small-curvature tunneling to calculate the rate constants for all four ethane reactions from 200 to 2000 K. The final MPW54 calculations are based on curvilinear-coordinate generalized-normal-mode analysis along the reaction path, and they include scaled frequencies and an anharmonic C–C bond torsion. They agree with experiment within 31% for 467–826 K except for a 38% deviation at 748 K; the results for the isotopologs are predictions since these rate constants have never been measured. The kinetic isotope effects (KIEs) are analyzed to reveal the contributions from subsets of vibrational partition functions and from tunneling, which conspire to yield a nonmonotonic temperature dependence for one of the KIEs. The stationary points and reaction-path potential of the MPW54 potential-energy surface are then used to parametrize a new kind of analytical potential-energy surface that combines a semiempirical valence bond formalism for the reactive part of the molecule with a standard molecular mechanics force field for the rest; this may be considered to be either an extension of molecular mechanics to treat a reactive potential-energy surface or a new kind of combined quantum-mechanical/molecular mechanical (QM/MM) method in which the QM part is semiempirical valence bond theory; that is, the new potential-energy surface is a combined valence bond molecular mechanics (CVBMM) surface. Rate constants calculated with the CVBMM surface agree with the MPW54 rate constants within 12% for 534–2000 K and within 23% for 200–491 K. The full CVBMM potential-energy surface is now available for use in variety of dynamics calculations, and it provides a prototype for developing CVBMM potential-energy surfaces for other reactions. © *2006 American Institute of Physics*.
[DOI: 10.1063/1.2132276]

I. INTRODUCTION

One of the ultimate goals of chemistry is to be able to understand and control chemical reaction systems. To realize this goal, one needs to determine the rates of chemical reactions. Thermochemical kinetics is the branch of theoretical chemistry that involves the prediction of the rate constants of chemical reactions by using information about the structures, energies, and vibrational frequencies (or vibrational free energies) of reactants and transition states,[1–3] along with estimates of nonsubstantial contributions[4] (such as tunneling or recrossing) to the free energy of activation. The present article presents an application of thermochemical kinetics to the reaction

$$H + C_2H_6 \rightarrow H_2 + C_2H_5. \qquad (R1)$$

The study of radical-molecule reactions is important in several application areas including combustion, atmospheric chemistry, interstellar chemistry, radiation chemistry, pyrolysis, polymer synthesis, photolysis, oxidation-reduction processes, and aging. The prototype hydrogen transfer reactions of H with CH_4 and C_2H_6 have been studied experimentally [CH_4 (Refs. 5–12) and C_2H_6 (Refs. 5, 6, 8, and 12–18)] and theoretically [CH_4(Refs. 12 and 19–55) and C_2H_6 (Refs. 12, 14, 23, and 56)]. The rate constant for $H+CH_4$ has now been calculated quite accurately. In particular, it was first shown that variational transition state theory[57,58] with multidimensional tunneling[58,59] VTST/MT contributions can reproduce quantum mechanical dynamical calculations for a given $H+CH_4$ potential-energy surface quite well. Then VTST/MT was applied in direct dynamics calculations with an accurate level of electronic structure theory to predict the rate constant and kinetic isotope effects.

Reaction (R1), in contrast, is still remarkably poorly

[a]Current address: Chemistry Department, University of Colorado at Denver, P.O. Box 173364, Denver, Colorado 80217.
[b]Electronic mail: truhlar@umn.edu

characterized. In 1936, Steacie and Phillips[5] experimentally estimated an activation energy E_a of 6.3 kcal/mol from measurements at room temperature, and in 1977, Jones *et al.*[16] measured 9.4 kcal/mol in experiments over the temperature range of 357–544 K. In 1988, Nicholas and Vaghjiani[18] estimated energy-dependent cross sections from photochemical experiments and thermally averaged them to obtain E_a=10.8 kcal/mol, which they judged to be "consistent" with the results of Jones *et al.* In 2001, Bryukov *et al.*[14] reported a measurement from 467 to 826 K that yielded E_a=8.6 kcal/mol. They could not measure the rate constant at higher temperatures because of dissociation of the radical product. They pointed out that extrapolation to lower and higher temperatures is needed for applications, but the extrapolations are quite ambiguous for a number of reasons. Attempts to extrapolate are uncertain not only because of the uncertainty in E_a but also because of the fact that Arrhenius plots are nonlinear.

Theoretical progress on direct calculations of the rate constant has also been marked by difficulties. In 2001, Senosiain *et al.*[56] modeled the available experimental data and reported an estimated barrier height of 9.7 kcal/mol. Their model also leads to an estimate of the transmission coefficient of 3.6 at 300 K. In contrast, the model of Bryukov *et al.* leads to an estimated barrier height of 9.1 kcal/mol; their rate constant extrapolated to room temperature exceeds the values measured there[5,16,18] by a factor of 3–4. Bryukov *et al.* concluded that "the low-temperature rate constant……remains uncertain."[14] A year later, one of these authors, Knyazev, returned to the problem with a more extensive computational study.[12] Based on isodesmic analyses, he estimated the barrier height at what he considered to be the highest level to be 8.9 kcal/mol (some other calculations[12] gave 9.0 kcal/mol). His extrapolated rate constant at 300 K is 1.2×10^{-17} cm^3 molecules^{-1} s^{-1}, which is a factor of 1.5×10^{-4} lower than the value at 600 K.[12] This compares to 9.4×10^{-17} cm^3 molecules^{-1} s^{-1} and a factor of 1.3×10^{-3} in the earlier paper.[14] The difference of an order of magnitude is disconcerting. Kerkeni and Clary[60] used a reduced-dimensionality quantum dynamics method in which two modes are treated in hyperspherical coordinates and the others are modeled using a harmonic approximation. Kerkeni and Clary's potential-energy surface has a classical barrier height of 13.5 kcal/mol and a zero-point-inclusive barrier height of 12.0 kcal/mol. In the present study, we will employ full-dimensional VTST/MT to investigate reaction (R1).

As part of the present study a potential-energy function (PEF) was constructed for $H+C_2H_6\rightarrow H_2+C_2H_5$ by combining semiempirical valence bond theory with molecular mechanics by dividing the entire system into a reactive part treated by quantum mechanics (QM) and a molecular mechanics (MM) part. This separation was motivated by a similar approach used in molecular-orbital-based combined QM/MM calculations[61,62] where one divides the system into a quantum-mechanical part treated by molecular orbital theory and a nonreactive part treated by molecular mechanics; we therefore call the new method the combined valence bond-molecular mechanics (CVBMM) method. For the present application, the VB part is based on the $H+CH_4\rightarrow H_2+CH_3$ surface of Joseph *et al.*[24] and related work by Raff[20] and Jordan and Gilbert,[30] and the MM part uses the standard MM3 (Refs. 63–66) force field. The CVBMM potential-energy surface is parametrized against density-functional theory (DFT) with a specific reaction parameter (SRP), which in turn is parametrized against a multicoefficient correlation method.

The rate constant calculations were performed by employing VTST/MT, in particular, canonical variational theory and the small-curvature tunneling (CVT/SCT) approximation. A key difference between reaction (R1) and the reaction of H with CH_4 is that there is a torsional mode in reaction (R1) that is not present in the $H+CH_4$ system. The importance of including anharmonicity in the torsion mode for this reaction was emphasized earlier by Senosiain *et al.*[56] and Sumathi *et al.*[43] We will therefore pay special attention to the effect of torsional anharmonicity on the calculated reaction rates.

The kinetic isotope effect (KIE) is a ratio of the rates of a chemical reaction when one or more atoms in one of the reactants is replaced by one of its isotopes. The study of KIEs is an active area in experimental and theoretical kinetics. Another objective of this study is to predict the rate constants and KIEs for the following reactions using direct dynamics calculations:

$$H + C_2D_6 \rightarrow HD + C_2D_5, \tag{R2}$$

$$D + C_2D_6 \rightarrow D_2 + C_2D_5, \tag{R3}$$

$$D + C_2H_6 \rightarrow DH + C_2H_5. \tag{R4}$$

These KIEs have apparently never been measured.

The analysis of Bryukov *et al.* was based on conventional transition state theory (TST) calculations without tunneling. Such calculations are inaccurate for two reasons. At low temperatures, conventional TST underestimates rate constants due to the fact that it does not include the quantum-mechanical tunneling effects. At high temperatures, conventional TST tends to overestimate rate constants because of trajectories recrossing a dividing surface through the saddle point at high temperatures. The VTST/MT method employed in the present study minimizes the recrossing effect by variationally optimizing the position of the dividing surface in coordinate space, and it also includes multidimensional quantum tunneling effects. This represents an improvement over Ref. 60 where only two modes were included in the tunneling dynamics; here 21 modes are included. VTST/MT is the most practical and the most accurate quantum-mechanical TST method, and it has been extensively validated.[40,48,67]

In this study, we not only carried out CVT/SCT calculations using CVBMM, we also carried out CVT/SCT calculations by direct dynamics. In the direct dynamics method,[25,40,59,68–72] all potential-energy surface (PES) information for each geometry is obtained from electronic structure calculations directly (without using a fit). In other words, the PES is implicitly defined by an electronic structure level that is used to provide energies, gradients, and Hessians to the dynamics calculations on the fly. We also use

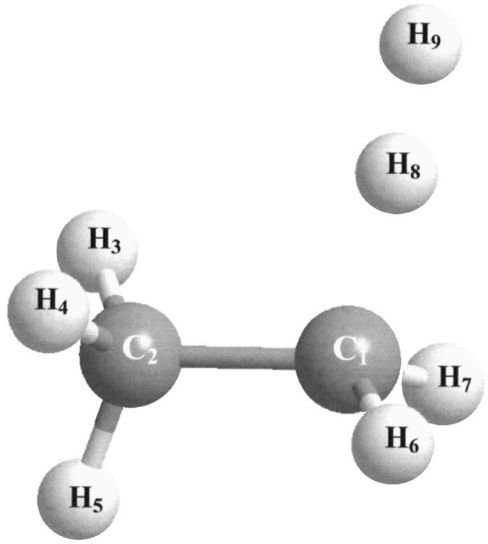

FIG. 1. Transition state geometry for the $H+C_2H_6 \rightarrow H_2+C_2H_5$ reaction.

a specific-reaction-parameter (SRP) approach[73] for the PES. The SRP method we used is called MPW*X*.[74] It is a one-parameter hybrid density-functional method.

The details of the CVBMM functional form of the potential-energy surface are given in Sec. II. Section III presents the CVT/SCT method that will be used for dynamics calculations. The high-level electronic structure methods used to estimate the barrier height and the DFT-SRP methods used to parametrize the CVBMM potential-energy surface are provided in Sec. IV. Section V provided the details of the software used for the calculations. In Secs. VI and VII we present the results and discussion. Section VIII contains concluding remarks.

II. CVBMM POTENTIAL-ENERGY SURFACE

In the CVBMM method, the potential energy V of the entire system is expressed as the sum of the potential energy V_{VB} of the reactive part, the potential energy V_{MM} of the molecular mechanics part, and the VB/MM interaction term:

$$V = V_{VB} + V_{MM} + V_{VB/MM}. \quad (1)$$

We will illustrate the method for reaction (R1), but it can be applied to a diverse range of reactions. Although potential-energy surfaces based on valence bond theory are available for many small-molecule reactions,[75–77] the method becomes unwieldy for larger molecules.[78,79] The CVBMM method allows one to combine convenient valence bond functional forms for a small reactive fragment with standard molecular mechanics[80,81] potentials for the nonreactive parts of the reactants in order to obtain analytical potential-energy functions suitable for calculating reactive dynamics.

For the $H+C_2H_6$ reaction, the reactive part consists of the attacking hydrogen atom labeled as H_9 in Fig. 1, the carbon atom (labeled as C_1) from which hydrogen is abstracted, and the three hydrogen atoms (labeled as H_6,H_7, and H_8) centered on this carbon. The MM part consists of the methyl group (labeled as C_2,H_3,H_4, and H_5) that is bonded to the reactive carbon atom. The molecular mechanics term is calculated using the MM3 force field.[63–66] The functional forms of the VB/MM interaction terms are constructed by introducing switching functions in the functional forms of the MM3 force field. A subset of parameters is changed from their original values in the V_{VB} and the $V_{VB/MM}$ functional forms to adjust the energy of reaction, the barrier height, the geometries, and the corresponding frequencies of reactant, products, and saddle point against the DFT calculation described in Sec. IV. The functional forms of the reactive and molecular mechanics terms are described in the rest of Sec. II, and the parametrization is discussed in Sec. VII.

II.A. Molecular mechanical terms

Molecular mechanics interactions are generally expressed in valence internal coordinates[82] such as bond lengths, bond angles, and torsional angles, and the potential energy is expressed in terms of bond stretching, angle bending, torsion, Coulomb, and van der Waals interactions. In the CVBMM method, in order to decide which interactions should be treated using MM, we use the same criterion that has been used successfully for other QM/MM calculations;[83] in particular, all interactions that involve at least one MM atom are treated using molecular mechanics terms. One of the limitations of molecular mechanics force fields is their inability to handle atoms and bonds that change their character as the reaction progresses. All molecular mechanics interaction that change their character during course of the reaction, i.e., appear or disappear, are treated as VB/MM interaction terms, whereas terms that retain that form (with or without geometry-dependent parameters) maybe in either V_{MM} or V_{VB}. In general, any interaction involving at least one MM and one VB atom is included in the $V_{VB/MM}$ term, and all interactions that do not involve any VB atom are treated using the molecular mechanics and are included in the V_{MM} term.

The MM3 force field[63–66] is used in the present paper to calculate all the molecular mechanics interactions. The details of MM3 are given in Refs. 63–66, and the equations relevant to the present work are summarized in the supporting information.[84]

In general V_{MM} contains the MM terms for all atoms in the MM subsystem. For the present reaction, V_{MM} contains three C–H stretches, three H–C–H bending terms, and stretch-bend and bend-bend cross terms. In general, an MM force field would also include Coulomb terms, but in the present example, the MM subsystem is a hydrocarbon fragment, and MM3 does not include Coulomb interactions for hydrocarbons. The relevant MM3 expressions used in the present paper are summarized in the supporting information.[84]

II.B. VB/MM interaction

Due to the difference in the bonding (i.e., connectivity pattern) between the reactant and products, there are some interactions that are present in the reactant but are absent in the product. According to the prescription that we include all MM interactions that involve at least one MM atom, $V_{VB/MM}$ contains the following interactions in either reactant or product: C–C stretch, H–C–C bend, H–C–C–H torsion, stretch-

bend interactions, bend-bend interactions, stretch-torsion cross terms, and van der Waals interactions. In the MM3 force field, all pairwise interactions except 1,2, and 1,3 interactions are included in the van der Waals terms.[66] To make the discussion concrete, we consider the abstraction of H_8 by H_9 in Fig. 1. The C–C–H bend term between H_8, C_1, and C_2 is present in ethane but absent in the ethyl radical since the C_1–H_8 bond is broken during the course of the reaction. The three H–C–C–H torsion terms associated with the H_8 hydrogen atom are other examples of interactions that are present in the reactant but absent in the product. The reactant and the product both include interaction of H_3, H_4, and H_5 with H_6, H_7, and H_8. Note that, as an additional simplification in the present work, all van der Waals interactions involving H_9 are not included.

In addition to interactions that appear or disappear as the reaction proceeds, other interactions are present all along the reaction path but with different parameters in reactants and products. For example, the equilibrium C–C distances for the reactant, saddle point, and the product obtained from the DFT calculations are 1.51, 1.50, and 1.48 Å, respectively. To extend the force field to treat such interactions, we have introduced two geometry-dependent switching functions T_1 and T_2. The first of these is defined as

$$T_1(r_{C_1H_i}) = 0.5(1 - \tanh[w_1(r_{C_1H_i} - w_2)]), \tag{2}$$

where w_1 and w_2 are adjustable parameters. Two MM3 parameters, one bend term, and three torsion terms are modulated by T_1. The reference C–C bond distance parameter and the reference C–C–H bond angle parameter are transformed smoothly from reactant to product using the equations

$$r^0_{CC,VB/MM} = P_1 r^0_{CC,R} + (1 - P_1) r^0_{CC,P}, \tag{3}$$

$$\theta^0_{CCH,VB/MM} = P_1 \theta^0_{CCH,R} + (1 - P_1) \theta^0_{CCH,P}, \tag{4}$$

where

$$P_1 = \prod_{i=6}^{8} T_1(r_{C_1H_i}). \tag{5}$$

Note that P_1 in the above equation is symmetric with respect to all three hydrogens that are initially bonded to C_1 atoms and goes to zero as one of the hydrogen atoms is abstracted. To emphasize the fact that the reference bond distance and bond angle are not constants (as they are in the MM3 force field) but depend on geometry, they are labeled as $r^0_{CC,VB/MM}$ and $\theta^0_{CCH,VB/MM}$, respectively. To annihilate the valence interactions that are present in the reactant (R) but are absent in the products (P), the corresponding MM3 terms are multiplied by the T_1 switching function.

The T_2 switching function is given by

$$T_2(\rho) = 0.5(1 - \tanh[w_3(\rho - w_4)]), \tag{6}$$

where w_3 and w_4 are adjustable parameters and ρ is a unitless quantity defined as

$$\rho = \frac{(r_{C_1H_6} + r_{C_1H_7} + r_{C_1H_8})}{3}\left(\frac{1}{r_{H_9H_6}} + \frac{1}{r_{H_9H_7}} + \frac{1}{r_{H_9H_8}}\right). \tag{7}$$

The geometry-dependent force constants are denoted by $k_{CC,VB/MM}$ and $k_{CCH,VB/MM}$, respectively, and are transformed using the T_2 switching function

$$k_{CC,VB/MM} = T_2 k_{CC,R} + (1 - T_2) k_{CC,P}, \tag{8}$$

$$k_{CCH,VB/MM} = T_2 k^{\theta}_{CCH,R} + (1 - T_2) k^{\theta}_{CCH,P}. \tag{9}$$

In the supporting information,[84] a term-by-term description is provided for all terms used in the evaluation of the $V_{VB/MM}$ energy.

II.C. Reactive part

The reactive part of the system is modeled using semiempirical valence bond theory. In particular, we modified the functional for the $H + CH_4 \rightarrow H_2 + CH_3$ potential-energy surface by Joseph *et al.*[24] and Jordan and Gilbert[30] which are based on older work by Raff.[20] These older functions are in turn based on functional forms based on the valence bond treatment of London.[75] Recently,[46] the parameters of Jordan and Gilbert surface were modified to give better agreement with the experimental results. Since construction of the CVBMM surface also involves reoptimization of the parameters of Jordan and Gilbert surface, the surface described in Ref. 46 was not used in the present work. The functional form of the CH_4 surface was defined by Jordan and Gilbert[30] in terms of C–H bond vectors. In the present work we used similar bond vectors that are defined as follows. The vectors $\mathbf{u}_1, \mathbf{u}_2$, and $\mathbf{u}_3$ are the three bond vectors along the C_1–H_6, C_1–H_7, and C_1–H_8 bonds, respectively. The bond vector $\mathbf{u}_4$ is defined as scaled a C–C bond vector and was obtained by multiplying the bond vector along the C_1–C_2 bond by the factor α_{scale}. The value of α_{scale} was obtained from the ratio of the C–C and C–H equilibrium bond distances in ethane. This yields $\alpha_{scale} = 0.717$. This treatment is identical to the scaling of C–C bonds in QM/MM calculations using a hydrogen link atom.[83] The magnitudes of the four vectors ($\mathbf{u}_i, i = 1, \ldots, 4$) are denoted as ($u_i, i = 1, \ldots, 4$).

To express the functional forms in a compact notation, the H_6–H_9, H_7–H_9, and H_8–H_9 internuclear distances are called $r_{HH,1}, r_{HH,2}$, and $r_{HH,3}$, respectively. The V_{VB} energy is written as a sum of stretching (str), out-of-plane (op) bending, and in-plane (ip) bending terms

$$V_{VB} = \sum_{i=1}^{3} V^{str}_{JG}(u_i, r_{C_1H_9}, r_{HH,i})\zeta(\rho) + V^{op}_{JG} + V^{ip}_{JG}, \tag{10}$$

where V^{str}_{JG} is a three-body London-Eyring-Polanyi-Sato (LEPS) function.[24] The expressions[20,24,30] for $V^{str}_{JG}, V^{op}_{JG}$, and V^{ip}_{JG} are presented in the supporting information.[84]

Note that each LEPS term involves three different kinds of interaction: C_1–H_i interactions with $i = 6, 7, 8$; H_i–H_9 interaction with $i = 6, 7, 8$; and C_1–H_9 interaction. The H_9 hydrogen atom does not form a bond with the C_1 carbon atom, and different Morse parameters were used by Schatz *et al.*[22] and Jordan and Gilbert[30] for C_1–H_9 and C_1–H_i ($i = 6, 7, 8$) interactions. The sets of Morse parameters for

C_1–H_9, C_1–H_i, and H_i–H_9 interactions are labeled as $({}^1D_{C_1H_9}, {}^3D_{C_1H_9}, \alpha_{C_1H_9}, r^0_{C_1H_9})$, $({}^1D_{CH}, {}^3D_{CH}, \alpha_{CH}, u^0)$, and $({}^1D_{HH}, {}^3D_{HH}, \alpha_{HH}, r^0_{HH})$, respectively. In the present functional form, the Morse parameters u^0, r^0_{HH}, and ${}^1D_{HH}$ were smoothly changed from reactant (R) to product (P) as follows:

$$u^0 = (1 - T_3)u^0_R + T_3 u^0_P, \tag{11}$$

$$r^0_{HH} = (1 - T_3)r^0_{HH,R} + T_3 r^0_{HH,P}, \tag{12}$$

$${}^1D_{HH} = (1 - T_3)\,{}^1D_{HH,R} + T_3\,{}^1D_{HH,P}, \tag{13}$$

where the switching function is defined as

$$T_3 = 0.5(1 - \tanh[w_5(\bar{u} - \bar{u}^0)]), \tag{14}$$

with w_5 as an adjustable parameter and

$$\bar{u} = \frac{1}{3}\sum_{i=1}^{3} u_i. \tag{15}$$

The term $\zeta(\rho)$ in Eq. (10) was not present in the original CH_4 surface and is a new modification for the present surface to provide more flexibility. It has the following form:

$$\zeta(\rho) = \sum_{i=1}^{6} \lambda_i g_i(\chi, d_i, \rho), \tag{16}$$

$$g_i(\chi, d_i, \rho) = e^{-\chi(\rho - d_i)^2}, \tag{17}$$

where χ, λ_i, and d_i are adjustable parameters.

III. VARIATIONAL TRANSITION STATE THEORY

III.A. Reaction-path potentials and rate constants

Detailed accounts of VTST are given elsewhere.[57,58,85–89] Here we summarize the key quantities used in the calculations. CVT is the version of VTST in which the transition state is optimized for a canonical ensemble. The CVT method as applied here minimizes the calculated rate constant at a given temperature as a function of the distance s along the reaction path of a sequence of dividing hypersurfaces [generalized transition states (GTSs)] transverse to the minimum-energy path (MEP) through an isoinertial coordinate system. The potential along the MEP is called $V_{MEP}(s)$, and adding the local zero-point energy to this yields the vibrationally adiabatic ground-state potential-energy curve $V_a{}^G(s)$. The value of $V_{MEP}(s)$ at the saddle point, relative to reactants, is called $V_f{}^{\neq}$ and relative to products is called $V_r{}^{\neq}$. The value of $V_a{}^G(s)$ at the saddle point, relative to reactants, is called $\Delta V_a{}^{G\neq}$. The value of $V_a{}^G(s)$ at products minus that at reactants is ΔH_0.

The CVT rate constant including multidimensional tunneling contributions used for the present study is

$$k^{CVT/SCT} = \kappa^{SCT}(T)k^{CVT}(T), \tag{18}$$

where k^{CVT} is the rate constant calculated by CVT (as explained in more detail in the supporting information[84]), and κ^{SCT} is the transmission coefficient used to include quantum effects on reaction coordinate motion, where the superscript stands for the SCT approximation.[59,89]

TABLE I. Energetics for the reaction $H+C_2H_6$(kcal/mol). $V_f^{\neq}$ is the forward classical barrier height, $V_r^{\neq}$ is the reverse classical barrier height, and ΔE is the classical energy of reaction.

Method	$V_f^{\neq}$	ΔE	$V_r^{\neq}$
	WFT		
G3SX[a]	12.21	−0.52	12.73
CBS-APNO[a]	11.54	−0.48	12.02
CBS-APNO[b]	11.55	−0.49	12.04
MC-QCISD/3[a]	12.33	−1.22	13.55
W1[a]	12.02	−0.55	12.57
W1[b]	12.05	−0.55	12.60
CCSD(T, full)/cc-pVTZ[c]	13.50	4.10	9.40
	WFT/DFT		
MCG3-MPWB[a]	11.44	−0.99	12.43
MCG3-MPWB[b]	11.42	−0.99	12.41
	DFT		
MPW54/6-31+G(d,p)	11.45	−0.43	11.88
MPW60/6-31+G(d,p)	11.98	−0.32	12.30
	Analytic		
CVBMM	11.45	−0.43	11.88
Experiment[d]	⋯	−0.43	⋯

[a]MC-QCISD/3 geometries are used.
[b]MPW B1K/MG3S geometries are used.
[c]MP2/c-pVTZ geometries are used. These calculations are from Ref. 60.
[d]Reference 102.

III.B. Hindered rotator approximation

In the $H+C_2H_6$ system, there is a vibrational mode corresponding to the torsional motion around the C–C bond. We treat this torsional mode by using a hindered rotator (HR) approximation scheme that was developed earlier.[90] In this HR treatment, the partition functions for the torsion are calculated by interpolation between the limits for harmonic oscillators and for free internal rotators. We use the RW scheme, where R denotes rectilinear and W denotes the internal rotation barrier (which is denoted W), proposed in a previous paper,[72] and we note that we showed recently that this RW scheme can give reasonable estimates of the ^{13}C KIEs for the $OH+CH_4$ reaction.[91] The internal rotation barrier W is calculated by a torsional scan with the MPW54 method. This yields $W=2.75$ kcal/mol for the reactant, and the value of W for the transition state is given in Sec. VI.D.

IV. ELECTRONIC STRUCTURE THEORY

IV.A. High-level methods

To obtain the energetics of reaction (R1), we performed several calculations using wave-function theory (WFT); in particular, we carried out G3SX,[92] MCG3-MPWB,[93] MC-QCISD/3,[94] W1,[95] and CBS-APNO[96] calculations to calculate the classical barrier height and energy of reaction. The results of these WFT calculations are compared to the results calculated by DFT in Tables I–IV. (The CVBMM results in Tables I, II, and IV will be explained in Sec. VII.)

TABLE II. ZPEs, differences in ZPE between saddle point and reactants and between saddle point and products, ground-state vibrationally adiabatic barrier height at the saddle point, and enthalpy of reaction (kcal/mol) at 0 K.

	ZPE						Energetics	
Method	C_2H_6	C_2H_5	H_2	SP	SP-*R*	SP-*P*	$\Delta V_a^{G\neq}$	ΔH_0
				WFT				
MC-QCISD/3	46.55	37.10	6.20	44.81	−1.74	1.50	10.59	−4.47
CCSD(T,full)/cc-pVTZ[a]	47.75	38.65	6.47	46.22	−1.53	1.09	12.00	1.50
				DFT				
MPW54/6-31+G(*d*,*p*)	45.82	36.44	6.15	44.22	−1.60	1.63	9.85	−3.65
MPW60/6-31+G(*d*,*p*)	45.64	36.30	6.12	44.02	−1.61	1.61	10.37	−3.54
				Analytic				
CVBMM	45.78	36.87	6.38	44.27	−1.50	1.03	9.95	−2.96

[a]MP2/c-pVTZ geometries are used.

IV.B. DFT

Another electronic structure method that we used in the present study is density-functional theory. The DFT calculations are based on a hybrid Fock-Kohn-Sham operator, which can be written as follows:[97,98]

$$F = F^H + (X/100)F^{\mathrm{HFE}} + (1 - X/100)(F^{\mathrm{SE}} + F^{\mathrm{GCE}}) + F^C, \tag{19}$$

where F^H is the Hartree operator (i.e., the nonexchange part of the Hartree-Fock operator), F^{HFE} is the Hartree-Fock exchange operator, X is the percentage of Hartree-Fock exchange, F^{SE} is Slater's local-density functional for exchange, F^{GCE} is the gradient correction for the exchange functional, and F^C is the correlation functional. When a modified Perdew-Wang (MPW) functional[99] is employed with 25% Hartree-Fock exchange ($X=25$) and the Perdew-Wang correlation functional (PW91),[100] this is MPW1PW91 in GAUSSIAN 03.[101] Using the 6-31+G(*d*,*p*) basis set, Lynch *et al.*[97] parametrized Eq. (19) with these choices of functionals against a database of barrier heights and energies of reactions. The resulting one-parameter method is called the MPW functional for kinetics, MPW1K in which $X=42.8$ (Refs. 42 and 97). Pu and Truhlar[45,48] also parametrized Eq. (19) with these functionals for the $H+CH_4$ reaction, yielding MPW60 for which $X=60$. The latter is called a SRP (Refs. 59 and 73) approach because the parameter is optimized for one reaction. In the next section we reoptimize X for reaction (R1).

TABLE III. Comparison of calculated barrier heights (kcal/mol) for $H+CH_4 \rightarrow H_2+CH_3$ and $H+C_2H_6 \rightarrow H_2+C_2H_5$ reactions.

	CH_4		C_2H_6		Difference	
Method	$V_f^{\neq}$	$V_r^{\neq}$	$V_f^{\neq}$	$V_r^{\neq}$	$\Delta V_f^{\neq}$	$\Delta V_r^{\neq}$
			WFT			
G3SX[a]	15.15	12.23	12.21	12.73	2.94	−0.50
CBS-APNO[a]	14.67	11.30	11.54	12.02	3.13	−0.72
MC-QCISD/3[a]	15.13	12.88	12.33	13.55	2.81	−0.67
W1[a,b]	14.88	11.89	12.02	12.57	2.86	−0.68
CCSD(T, full)/cc-pVTZ[c]	15.48	11.78	13.50	9.40	1.98	2.38
			DFT			
MPW54/DIDZ[d]	14.34	10.86	11.45	11.88	2.89	−1.02
MPW60/DIDZ[d]	14.80	11.10	11.98	12.30	2.82	−1.20
			WFT/DFT			
MCG3-MPWB[a]	14.46	11.62	11.44	12.43	3.02	−0.80

[a]For the G3SX, CBS-APNO, MC-QCISD/3, W1, and MCG3-MPWB calculations, the QCISD/MG3 geometries are used for the $H+CH_4$ reaction, and MC-QCISD/3 geometries are used for the $H+C_2H_6$ reaction. Note that the QCISD/MG3 geometries are very close to the MC-QCISD/3 ones.
[b]The W1 results for the $H+CH_4$ are taken from Ref. 115.
[c]The MP2(full)/cc-pVTZ geometries are used for the CCSD(T, full)/cc-pVTZ calculation and the results are taken from Refs. 60 and 116.
[d]For the MPW54 and MPW60 DFT methods, the consistently optimized geometries are used for each level of theory.

TABLE IV. Geometries and imaginary frequencies for the saddle point. Distances are in Å, bond angles are in deg, and frequencies are in cm^{-1}.

	Bond lengths			Bond angle		
Method	H–H	C–H	Sum	∠C–H–H	∠H–C–C–H	Imaginary frequency
			WFT			
MP2(full)/cc-pVTZ[a]	0.866	1.417	2.283	178	180	1498*i*
QCISD/6-311++G(2*df*,2*p*)	0.925	1.355	2.280	177	180	…
MC-QCISD/3	0.924	1.354	2.278	176	180	1474*i*
			DFT			
MPW54/6-31+*G*(*d*,*p*)	0.912	1.355	2.267	178	180	1359*i*
MPW60/6-31+*G*(*d*,*p*)	0.912	1.353	2.265	177	180	1392*i*
			WFT/DFT			
MCG3-MPWB[b]	0.924	1.354	2.278	176	180	1474*i*
			Analytic			
CVBMM	0.922	1.355	2.277	179	180	1537*i*

[a]Reference 60.
[b]Reference 93.

IV.C. Parametrization of the DFT-SRP functional

A general scheme to improve the accuracy of the one-parameter DFT surfaces for a specific reaction is to vary the percentage of HF exchange so that the predicted surface provides a better representation for the specific reaction of interest. Recently we[102] have shown that the 6-31+G(*d*,*p*) (Ref. 103) basis set can provide useful accuracy for energies of reaction and reaction barrier height with DFT methods. Thus, we used 6-31+G(*d*,*p*) basis set with the MPW*X* for reaction (R1). (In general, MPW*X* denotes the functional obtained as in the previous subsection but for a given percentage *X* of Hartree-Fock exchange.) We adjust the value of *X* in Eq. (19) so that the MPW*X* method yields an energy of reaction equal to experimental value, −0.43 kcal/mol, for the reaction (R1). [This experimental energy of reaction is obtained from the MGAE109/05 (Refs. 93 and 94) database of zero-point-exclusive experimental atomization energies.] This yields a new DFT-SRP functional, MPW54, that has 54% Hartree-Fock exchange.

V. SOFTWARE

The W1 calculations were carried out with the MOLPRO program.[104] The G3SX and MCG3-MPWB calculations were performed with the MLGAUSS (Ref. 105) program in conjunction with the GAUSSIAN03 (Ref. 101) program. The calculation of $k^{CVT/SCT}$ reported below was performed using GAUSSRATE (Ref. 106) which interfaces the VTST/MT program POLYRATE (Ref. 107) to the electronic structure program GAUSSIAN03.[101] The GAUSSRATE, MLGAUSS, and POLYRATE programs can be downloaded from the Truhlar's software webpage.[108] The CVBMM potential-energy surface is available in POTLIB.[109,110]

VI. RESULTS FROM DIRECT DYNAMICS CALCULATIONS

VI.A. Details of the calculations

In the dynamics calculations, the scaling mass for all coordinates is set equal to 1 amu. The MEP in the isoinertial coordinate system is followed by the Page-McIver algorithm.[111] The gradient step size is $0.005a_0$ and the Hessian is calculated every nine steps. We scaled all DFT vibrational frequencies along the reaction coordinate, in particular, we used 0.9415 as the scaling factor for the MPW54/6-31+G(*d*,*p*) method and 0.9312 for MPW60/6-31+G(*d*,*p*). These scaling factors were optimized against the ZPE13/99 database,[112] which is a database of 13 anharmonic vibrational zero-point energies (ZPEs). The coordinate system for the generalized-normal-mode analysis along the reaction path is a set of redundant curvilinear internal coordinates.[113]

VI.B. Energetics

Table I is the summary of the energetics calculated by different methods. The barrier heights calculated by the G3SX, CBS-APNO, MC-QCISD/3, W1, MCG3-MPWB, and MPW*X* methods are in good agreement with one another, but they are lower than the barrier height from Kerkeni and Clary's CCSD(T)/cc-pVTZ//MP2/cc-pVTZ calculation by about 2 kcal/mol. Rate constants that are calculated with the PES based on the CCSD(T)/cc-pVTZ calculations by Kerkeni and Clary are therefore much lower than the experimental rate constant. This is an indication that Kerkeni and Clary's[60] CCSD(T)/cc-pVTZ calculation overestimates the barrier height of the reaction (R1). The barrier height obtained by the MPW60/6-31+G(*d*,*p*) method of Pu *et al.*[40] is close to the W1 calculation. The DFT-SRP method developed in this study, MPW54/6-31+G(*d*,*p*), gives a similar barrier height to that from the MCG3-MPWB method. Table II lists the zero point energies, vibrationally adiabatic

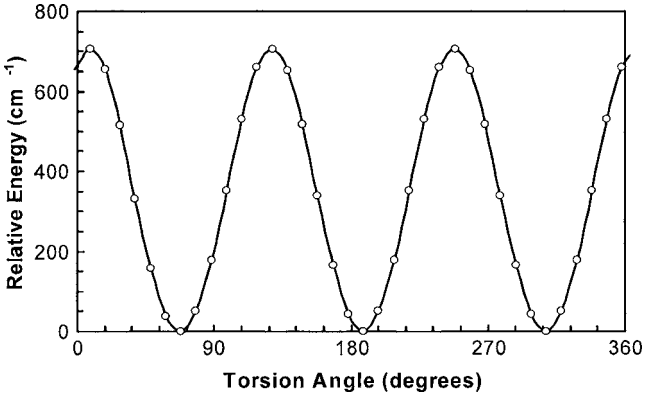

FIG. 2. Rotational barrier (in cm^{-1}) of the transition state for the $H+C_2H_6 \rightarrow H_2+C_2H_5$ reaction at the MPW54/6-31+G(d,p) level.

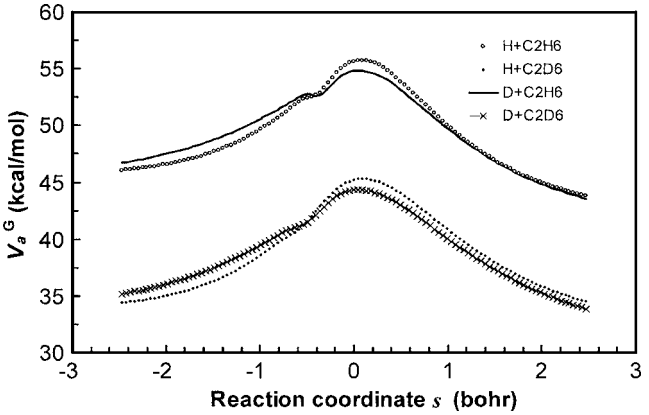

FIG. 3. V_a^G for the four reactions as a function of reaction coordinate s obtained using the MPW54/6-31+G(d,p) level with the HR approximation.

ground-state barrier height, and enthalpy of reaction. Table III gives a comparison of the calculated forward ($V_f^{\neq}$) and reverse ($V_r^{\neq}$) barrier heights for $H+CH_4$ and $H+C_2H_6$ reactions using various[92–96] high-level methods. Table III shows that G3SX, CBS-APNO, W1, and MCG3-MPWB give similar barrier heights and a similar trend in the difference between the two reactions, but the CCSD(T, full) method without extrapolation is unreliable.

VI.C. Transition state geometries and imaginary frequencies

Table IV gives the key geometric parameters of the transition state, which include the length of the breaking bond (C–H) and that of the forming bond (H–H) in the transition state of $H+C_2H_6$, and their sum is also included in the table; this quantity is called perpendicular looseness, and it measures the looseness of the transition state structure in a direction perpendicular to the reaction coordinate.[42] In our previous work, the MC-QCISD/3 method has proven to be able to provide accurate geometries for stable molecules[114] and for transition states.[112]

From Table IV, we can see that MC-QCISD/3 gives a very similar transition state geometry to that obtained by the QCISD/6-311++G$(2df,2p)$ method. If we use the MC-QCISD/3 geometry as a reference, the MP2/cc-pVTZ method gives a shorter H–H bond (forming bond) and a longer C–H bond (breaking bond), whereas MPW54 and MPW60 give more accurate transition state geometries.

VI.D. Torsional potential

The lowest-frequency mode of the reactant is an internal rotation. The torsional barrier height for the reactant is 2.86 and 2.88 kcal/mol at MPW54/6−31+G(d,p) and MPW60/6−31+G(d,p) level, respectively. These values are in good agreement with the experimental barrier height of

TABLE V. Direct dynamics rate constants ($cm^3\,molecule^{-1}\,s^{-1}$) for the $H+C_2H_6$ reaction. The 6-31+G(d,p) basis set used. HO denotes the harmonic-oscillator approximation for all modes; HR denotes that the lowest-frequency mode is treated as a hindered rotator.

	MPW60 (HO)			MPW54 (HO)			MPW54 (HR)			
T (K)	TST	CVT	CVT/SCT	TST	CVT	CVT/SCT	TST	CVT	CVT/SCT	Exp.
200	4.76*E*−22	4.00*E*−22	1.78*E*−19	1.77*E*−21	1.44*E*−21	5.29*E*−19	1.66*E*−21	1.29*E*−21	4.77*E*−19	NA
300	3.05*E*−18	2.77*E*−18	3.20*E*−17	7.29*E*−18	6.50*E*−18	7.62*E*−17	6.87*E*−18	5.90*E*−18	6.96*E*−17	NA
400	2.68*E*−16	2.53*E*−16	9.16*E*−16	5.14*E*−16	4.80*E*−16	1.81*E*−15	4.84*E*−16	4.37*E*−16	1.66*E*−15	NA
467	1.92*E*−15	1.85*E*−15	4.61*E*−15	3.36*E*−15	3.20*E*−15	8.28*E*−15	3.31*E*−15	3.06*E*−15	8.01*E*−15	1.04*E*−14
491	3.45*E*−15	3.33*E*−15	7.55*E*−15	5.86*E*−15	5.60*E*−15	1.32*E*−14	5.49*E*−15	5.10*E*−15	1.21*E*−14	1.42*E*−14
534	8.69*E*−15	8.43*E*−15	1.67*E*−14	1.41*E*−14	1.36*E*−14	2.78*E*−14	1.32*E*−14	1.24*E*−14	2.56*E*−14	2.86*E*−14
586	2.25*E*−14	2.20*E*−14	3.84*E*−14	3.50*E*−14	3.40*E*−14	6.10*E*−14	3.26*E*−14	3.09*E*−14	5.61*E*−14	5.45*E*−14
600	2.82*E*−14	2.75*E*−14	4.69*E*−14	4.35*E*−14	4.26*E*−14	7.36*E*−14	3.97*E*−14	3.86*E*−14	6.79*E*−14	NA
612	3.42*E*−14	3.35*E*−14	5.58*E*−14	5.22*E*−14	5.09*E*−14	8.67*E*−14	4.85*E*−14	4.62*E*−14	7.96*E*−14	7.88*E*−14
637	4.98*E*−14	4.89*E*−14	7.80*E*−14	7.47*E*−14	7.30*E*−14	1.19*E*−13	6.93*E*−14	6.61*E*−14	1.09*E*−13	1.08*E*−13
693	1.06*E*−13	1.04*E*−13	1.54*E*−13	1.53*E*−13	1.50*E*−13	2.26*E*−13	1.41*E*−13	1.36*E*−13	2.07*E*−13	2.21*E*−13
748	2.00*E*−13	1.98*E*−13	2.76*E*−13	2.82*E*−13	2.78*E*−13	3.92*E*−13	2.59*E*−13	2.50*E*−13	3.58*E*−13	2.59*E*−13
776	2.69*E*−13	2.67*E*−13	3.62*E*−13	3.74*E*−13	3.70*E*−13	5.07*E*−13	3.43*E*−13	3.32*E*−13	4.62*E*−13	4.40*E*−13
796	3.29*E*−13	3.26*E*−13	4.36*E*−13	4.53*E*−13	4.48*E*−13	6.04*E*−13	4.15*E*−13	4.02*E*−13	5.50*E*−13	4.45*E*−13
826	4.36*E*−13	4.33*E*−13	5.67*E*−13	5.95*E*−13	5.88*E*−13	7.74*E*−13	5.42*E*−13	5.27*E*−13	7.04*E*−13	5.36*E*−13
1000	1.69*E*−12	1.68*E*−12	2.01*E*−12	2.17*E*−12	2.16*E*−12	2.58*E*−12	1.95*E*−12	1.90*E*−12	2.31*E*−12	NA
1500	1.75*E*−11	1.75*E*−11	1.86*E*−11	2.06*E*−11	2.06*E*−11	2.20*E*−11	1.75*E*−11	1.75*E*−11	1.86*E*−11	NA
2000	6.62*E*−11	6.62*E*−11	6.80*E*−11	7.45*E*−11	7.45*E*−11	7.66*E*−11	6.03*E*−11	5.96*E*−11	6.23*E*−11	NA

TABLE VI. Direct dynamics rate constants (cm^3 $molecule^{-1}$ s^{-1}) for the $H+C_2D_6$, $D+C_2D_6$, and $D+C_2H_6$ reactions All calculations in this table use the MPW 54/6-31+G(d,p) electronic structure level and use the HR approximation for the lowest-frequency mode.

	$H+C_2D_6$			$D+C_2D_6$			$D+C_2H_6$		
T (K)	TST	CVT	CVT/SCT	TST	CVT	CVT/SCT	TST	CVT	CVT/SCT
200	6.48$E-23$	5.26$E-23$	2.75$E-21$	3.22$E-22$	3.03$E-22$	1.19$E-20$	8.41$E-21$	8.06$E-21$	7.35$E-19$
300	8.24$E-19$	7.05$E-19$	2.83$E-18$	2.00$E-18$	1.93$E-18$	7.90$E-18$	1.80$E-17$	1.75$E-17$	1.33$E-16$
400	1.01$E-16$	9.11$E-17$	1.86$E-16$	1.79$E-16$	1.75$E-16$	3.68$E-16$	9.30$E-16$	9.14$E-16$	2.88$E-15$
491	1.56$E-15$	1.45$E-15$	2.29$E-15$	2.36$E-15$	2.33$E-15$	3.76$E-15$	9.01$E-15$	8.90$E-15$	1.91$E-14$
600	1.48$E-14$	1.41$E-14$	1.89$E-14$	1.99$E-14$	1.97−E14	2.70$E-14$	5.94$E-14$	5.89$E-14$	9.8$E-14$
612	1.81$E-14$	1.73$E-14$	2.29$E-14$	2.42$E-14$	2.39$E-14$	3.24$E-14$	7.05$E-14$	6.99$E-14$	1.14$E-13$
748	1.18$E-13$	1.14$E-13$	1.37$E-13$	1.45$E-13$	1.44$E-13$	1.76$E-13$	3.49$E-13$	3.47$E-13$	4.82$E-13$
1000	1.10$E-12$	1.08$E-12$	1.19$E-12$	1.25$E-12$	1.24$E-12$	1.39$E-12$	2.45$E-12$	2.44$E-12$	2.93$E-12$
1500	1.22$E-11$	1.21$E-11$	1.25$E-11$	1.30$E-11$	1.30$E-11$	1.36$E-11$	2.15$E-11$	2.14$E-11$	2.33$E-11$
2000	4.66$E-11$	4.62$E-11$	4.70$E-11$	4.86$E-11$	4.85$E-11$	4.97$E-11$	7.50$E-11$	7.46$E-11$	7.81$E-11$

2.88 kcal/mol.[64] Figure 2 presents the torsional potential for the transition state of reaction (R1) at the MPW54/6-31 +G(d,p) level of theory. The barrier associated with the internal rotation at the transition state is 2.02 kcal/mol for the MPW54 surface and 2.04 kcal/mol for the MPW60 surface. All generalized transition states in the HR calculations used the value of the torsional barrier at the saddle point for that potential energy surface.

VI.E. Barrier shape

Figure 3 presents the adiabatic ground-state potential curve $V_a^G(s)$ for reactions (R1)–(R4). The shoulders in Fig. 3 result from competition between a decreasing potential energy and an increasing zero-point contribution as the system moves away from the saddle point. The Born-Oppenheimer potential along the MEP for reactions (R1)–(R4) is provided in the supporting information.[84]

VI.F. Reaction-rate constants

Reaction-rate constants obtained from dynamical calculations and corresponding experimental values for the $H+C_2H_6$ reaction are given in Table V. We compared three different dynamics calculations, in particular, calculations based on MPW60/6-31+G(d,p) and MPW54/6-31+G(d,p) surfaces with the harmonic approximation and one based on the MPW54/6-31+G(d,p) surface with hindered rotator anharmonicity. To analyze the variational and tunneling effects, we list rate constants for conventional TST, for canonical variational transition state theory (CVT), and for CVT with multidimensional tunneling contributions calculated in the small-curvature tunneling (CVT/SCT) approximation.

If we compare the CVT/SCT harmonic rate constants at 637 K, we see that rate constant from the MPW60 surface with the harmonic approximation underestimates the rate constant by 28% and that from the MPW54 surface overestimates it by 10%. The HR approximation lowers the CVT/SCT rate constant, and the rate constant from the MPW54 surface with the HR approximation agrees well with experiment. More broadly the mean absolute deviation from experiment at the 11 temperatures from 467 to 826 K is only 15%, and the mean deviation is only+4%. These deviations are within the experimental uncertainty. The maximum deviation from experiment is 38% at 748 K, and the second largest deviation is 31% at 826 K.

The difference between the TST and CVT values is a measure of how much recrossing occurs at the conventional transition state and can be recovered by variational optimization of the transition state. For the MPW54(HR) calculation, Table V shows that variational optimization of the tran-

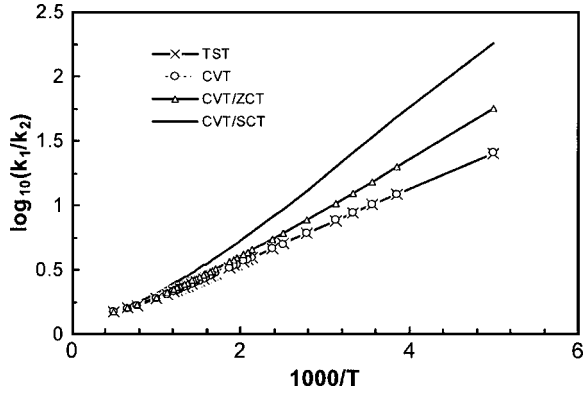

FIG. 4. Logarithm of the deuterium KIE for reactions (R1) and (R2) vs $1000/T$ obtained using the MPW54/6-31+G(d,p) level with the HR approximation. k_1 is for $H+C_2H_6$ and k_2 is for $H+C_2D_6$.

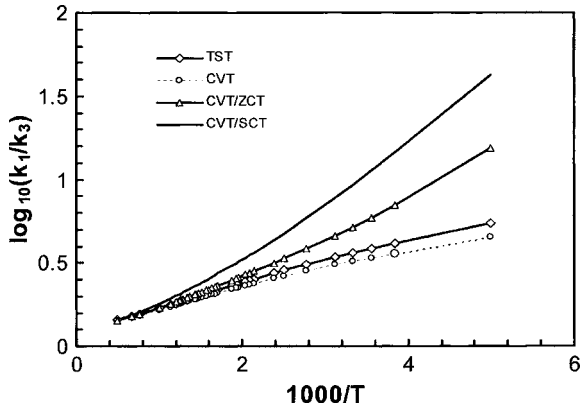

FIG. 5. Logarithm of the deuterium KIE for reactions (R1) and (R3) vs $1000/T$ obtained using the MPW54/6-31+G(d,p) level with the HR approximation. k_1 is for $H+C_2H_6$ and k_3 is for $D+C_2D_6$.

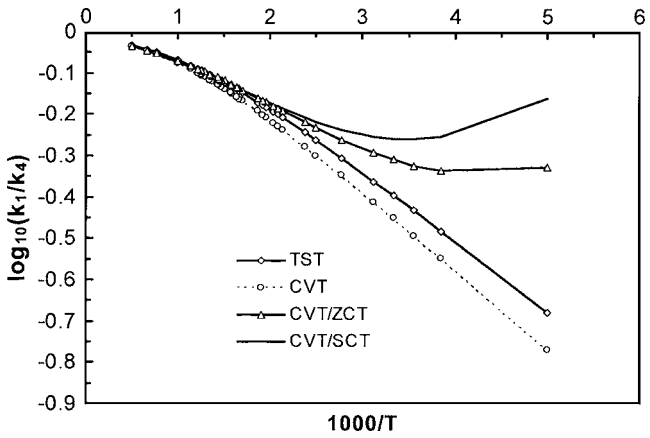

FIG. 6. Logarithm of the deuterium KIE for reactions (R1) and (R4) vs $1000/T$ obtained using the MPW54/6-31+G(d,p) level with the HR approximation. k_1 is for $H+C_2H_6$ and k_4 is for $D+C_2H_6$.

sition state location reduces the rate constant for H transfer by 22% at 200 K, 7%–14% at 300–491 K, and 6% or less for 534–2000 K. The net effect of the tunneling and nonclassical reflection contributions increases the CVT rate constant by factors of 370, 12, and 3.8 at 200, 300, and 400 K, respectively, by 65% at 637 K, by 22% at 1000 K, and by 5% at 2000 K.

The rate constants calculated by using conventional TST with one-dimensional Wigner tunneling (TST/W) for the MPW54/6-31+G(d,p) surface are given in the supporting information.[84]

VI.G. Kinetic isotope effects

The KIE is defined as the ratio k_i/k_j, where k_i is the rate constant for the isotopic reaction with lighter mass, and k_j is the rate constant for the corresponding heavier isotopic reaction. KIEs greater than 1 are called "normal," and those less than 1 are called "inverse." Table VI lists the rate constants for reactions (R2)–(R4), and Fig. 4–6 are the plots of temperature dependences of KIEs. Figures 4 and 5 show that the KIEs for $H+C_2H_6/H+C_2D_6$ and $H+C_2H_6/D+C_2D_6$ are normal and monotonically decreasing with increasing temperature. Figure 6 shows that $H+C_2H_6/D+C_2H_6$ shows an inverse KIE.

The CVT/SCT KIE for $H+C_2H_6/D+C_2H_6$ shows a nonmonotonic temperature dependence. At high temperatures, the KIE increases with increasing temperatures, whereas at low temperatures, it decreases with increasing temperature. To explain this phenomenon, we performed a factorization analysis for the KIEs of $H+C_2H_6/D+C_2H_6$. The factors are listed in Table VII, which shows that the CVT KIE is monotonically increasing (with increasing temperature) due to $\eta_{\mathrm{vib,mid}}$. From an analysis of the contributions to $\eta_{\mathrm{vib,mid}}$ from each of the modes, we found that the main contribution is from the quasisymmetric stretch mode of the forming bond and breaking bond. Table VII also shows that the tunneling contribution η_{tun} tends to increase the KIEs at low temperatures. The interplay of $\eta_{\mathrm{vib,mid}}$ and η_{tun} produces the nonmonotonic temperature dependence.

VII. PARAMETRIZATION OF THE CVBMM POTENTIAL-ENERGY SURFACE

Geometry dependence in the reference C–C bond distance and the reference C–C–H bond angle is introduced by using Eqs. (3) and (4). The force constants for the C–C stretch and C–C–H bend are varied as shown in Eqs. (8) and (9), respectively. The parameters $w_1,\ldots,w_5$ are optimized to give the correct frequencies and geometries at the saddle point. The parameters w_1 and w_2 control the rate of switching of the T_1 and T_2 switching functions. It was found that using a fast switching rate for the force constants would introduce a spurious shoulder near the saddle point in the ground-state adiabatic potential-energy curve, and therefore the force constants were switched more slowly than the bond distances to avoid this. One of the major differences between the $H+CH_4$ and the $H+C_2H_6$ reactions is the exothermicity of the two reactions. The methane reaction is endothermic while the ethane reaction is exothermic. The ${}^1D_{\mathrm{HH}}$ Morse parameter in the product region is optimized to get the correct exothermicity. The reference bond distances of Eqs. (11) and (12) are also changed as the reaction progresses from reactants to products. The scaling function $\zeta(\rho)$ in Eq. (10) was obtained by least-squares calculation minimizing the root-mean-square (rms) deviation in energies along the minimum-energy path obtained using MPW 54/6-31+G(d,p). This was crucial to get the correct shape and the width of the barrier. All other parameters are fixed at the literature values.[30] The parameters used in the CVBMM surface are given in the supporting information.[84]

TABLE VII. KIEs and factors for the $H+C_2H_6/D+C_2H_6$. All calculations in this table use the MPW 54/6-31 +G(d,p) electronic structure level with the HR approximation for the torsion mode.

			η_{vib}							
T (K)	η_{trans}	η_{rot}	$\eta_{\mathrm{vib,high}}$	$\eta_{\mathrm{vib,mid}}$	$\eta_{\mathrm{vib,low}}$	$\eta_{\mathrm{vib,tot}}$	η_{pot}	η^{CVT}[a]	η_{tun}	$\eta^{\mathrm{CVT/SCT}}$
200	2.69	0.78	0.99	0.09	0.68	0.06	1.37	0.17	4.05	0.69
250	2.69	0.78	0.99	0.14	0.69	0.10	1.28	0.26	2.13	0.56
300	2.69	0.78	0.99	0.19	0.70	0.14	1.21	0.36	1.56	0.55
400	2.69	0.78	1.00	0.29	0.72	0.20	1.15	0.48	1.18	0.60
491	2.69	0.78	1.00	0.35	0.72	0.25	1.09	0.59	1.11	0.66
600	2.69	0.78	1.00	0.47	0.71	0.33	1.01	0.73	1.01	0.73
1500	2.69	0.78	1.00	0.60	0.71	0.43	1.00	0.90	1.00	0.90

[a] $\eta^{\mathrm{CVT}}=\eta_{\mathrm{trans}}\eta_{\mathrm{rot}}\eta_{\mathrm{vib}}\eta_{\mathrm{pot}}$.

TABLE VIII. Optimized geometries of the stationary points for the $H+C_2H_6$ reaction obtained from the CVBMM potential-energy surface. Distances are in Å and angles are in deg.

	C_2H_6	Saddle point	C_2H_5
C_1–C_2	1.51	1.50	1.48
C_1–H_8	1.09	1.36	···
C_1–H_7	1.09	1.08	1.08
H_8–H_9	···	0.922	0.736
H_8–C_1–H_7	108	104	···
H_8–C_1–C_2	111	110	···
H_7–C_1–C_2	111	115	119
H_9–H_8–C_1	···	179	···

VII.A. Energetics and geometries

The geometries of the reactant, products, and the saddle point are in good agreement with the MPW 54/6-31+G(d,p) calculations. Table VIII lists the optimized geometries of the reactant, products, and the saddle point obtained from the CVBMM potential-energy surface. The energy of reaction and the barrier height obtained from the CVBMM potential-energy surface are in good agreement with the MPW 54/6-31 +G(d,p) calculations, as shown in Table I. The torsional barrier height at the saddle point in the CVBMM potential-energy surface is found to be 2.14 kcal/mol and is in good agreement with MPW54 value (higher by only 0.12 kcal/mol). For ethane the torsional barrier height is 2.44 kcal/mol in the CVBMM surface and is similar to MM3 torsional barrier of 2.41 kcal/mol

VII.B. Frequencies

Table IX lists the vibrational frequencies of the reactant, products, and the saddle point obtained at the optimized geometries from the CVBMM potential-energy surface. The mean-signed error (MSE) and the mean-unsigned error (MUE) in the frequencies of the bound vibrational modes between scaled MPW 54/6-31+G(d,p) and the CVBMM surface are 2 and 50 cm^{-1} for ethane, −27 and 49 cm^{-1} for ethyl radical, and −2 and 68 cm^{-1} for saddle-point geometries. The frequency in the CVBMM surface associated with the unbound mode at the saddle point is 176 cm^{-1} higher than the MPW54 value.

TABLE IX. Normal-mode analysis of the stationary points of the CVBMM potential-energy surface of the $H+C_2H_6$ reaction.

	Frequency (cm^{-1})			
H_2	4424			
C_2H_5	127	532	974	981
	1042	1189	1490	1498
	1503	1542	2880	2963
	2964	3056	3161	
C_2H_6	292	949	949	972
	1107	1107	1405	1464
	1464	1467	1491	1491
	2873	2963	2963	3005
	3029	3029		
Saddle point	1537i	211	402	646
	848	936	962	1114
	1166	1299	1327	1379
	1397	1401	1472	1581
	2803	2884	2885	3105
	3150			

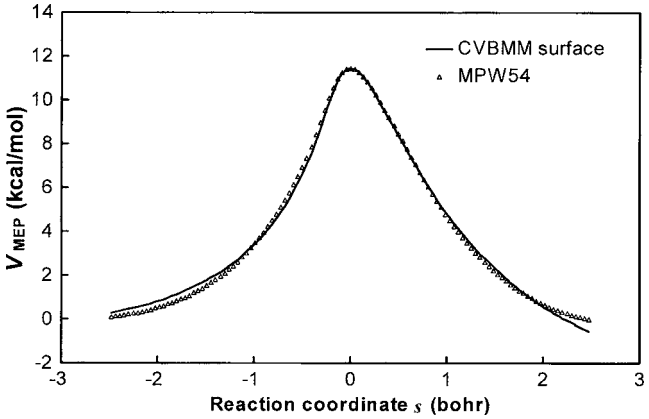

FIG. 7. Comparison of the plot of V_{MEP} for the $H+C_2H_6$ reaction as a function of reaction coordinate s obtained by using the CVBMM surface and the MPW54/6-31+G(d,p) level.

VII.C. Barrier shape and rate constants

The V_{MEP} and V_a^G curves obtained from the CVBMM surface are shown in Figs. 7 and 8, respectively; they are in good agreement with the MPW54 calculations. Note that the generalized-normal-mode frequencies along the minimum-energy path for the CVBMM surface are in good agreement with MPW54 calculations and are responsible for giving good agreement in the V_a^G curves. In the dynamics calculations, the scaling mass for all coordinates is set equal to 1 amu. The MEP is followed by the Page-McIver algorithm[111] with a gradient step size of 0.005 a_0. Since the CVBMM surface is optimized against the scaled MPW 54/6-31 +G(d,p) frequencies, a frequency-scale factor of 1.0 is used for the rate constant calculations. The reaction-rate constants calculated using the CVBMM surface are listed in Table X along with the MPW 54/6-31+G(d,p) results. The average

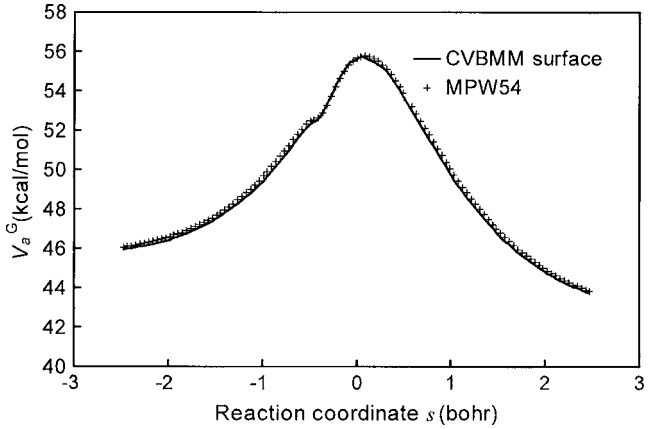

FIG. 8. Comparison of the plot of V_a^G for the $H+C_2H_6$ reaction as a function of reaction coordinate s obtained by using the CVBMM surface and the MPW54/6-31+G(d,p) level.

TABLE X. Rate constants (cm^3 $molecule^{-1}$ s^{-1}) obtained using the CVBMM surface for the $H+C_2H_6$ reaction.

T(K)	TST	CVT	CVT/SCT	Expt.
200	1.25×10^{-21}	1.24×10^{-21}	1.90×10^{-18}	NA
300	5.20×10^{-18}	5.20×10^{-18}	1.44×10^{-16}	NA
400	3.63×10^{-16}	3.63×10^{-16}	2.40×10^{-15}	NA
467	2.35×10^{-15}	2.35×10^{-15}	9.48×10^{-15}	1.04×10^{-14}
491	4.09×10^{-15}	4.08×10^{-15}	1.45×10^{-14}	1.42×10^{-14}
534	9.81×10^{-15}	9.80×10^{-15}	2.86×10^{-14}	2.86×10^{-14}
586	2.42×10^{-14}	2.41×10^{-14}	5.89×10^{-14}	5.45×10^{-14}
600	3.00×10^{-14}	3.00×10^{-14}	7.03×10^{-14}	NA
612	3.60×10^{-14}	3.59×10^{-14}	8.14×10^{-14}	7.88×10^{-14}
637	5.13×10^{-14}	5.12×10^{-14}	1.09×10^{-13}	1.08×10^{-13}
693	1.05×10^{-13}	1.04×10^{-13}	1.98×10^{-13}	2.21×10^{-13}
748	1.92×10^{-13}	1.91×10^{-13}	3.32×10^{-13}	2.59×10^{-13}
776	2.54×10^{-13}	2.53×10^{-13}	4.22×10^{-13}	4.40×10^{-13}
796	3.07×10^{-13}	3.06×10^{-13}	4.97×10^{-13}	4.45×10^{-13}
826	4.02×10^{-13}	4.00×10^{-13}	6.28×10^{-13}	5.36×10^{-13}
1000	1.45×10^{-12}	1.44×10^{-12}	1.96×10^{-12}	NA
1500	1.36×10^{-11}	1.35×10^{-11}	1.54×10^{-11}	NA
2000	4.89×10^{-11}	4.84×10^{-11}	5.20×10^{-11}	NA

percent deviation of the CVBMM rate constants from the MPW 54/6-31+G(d,p) ones is calculated using the formula:

$$\text{average \% deviation} = \frac{1}{18}\sum_{i=1}^{18}\left|\frac{k^{\text{CVBMM}}-k^{\text{MPW54}}}{k^{\text{MPW54}}}\right|\times 100, \tag{20}$$

and the values for TST, CVT, and CVT/SCT are 31%, 29%, and 33%, respectively.

The rate constants calculated by using conventional TST with one-dimensional Wigner tunneling (TST/W) for the CVBMM surface are given in the supporting information.[84]

VIII. CONCLUDING REMARKS

In this work, we developed an analytical CVBMM surface for the $H+C_2H_6$ abstraction reaction. We performed variational transition state theory calculations with multidimensional tunneling to calculate rate constants and KIEs using both direct dynamics and the new CVBMM potential-energy surface. The CVBMM method provides a systematic procedure for classifying vibrational interactions and is a general method for fitting analytical potential-energy surfaces that can be applied to larger systems. For example, applying the CVBMM method to $H+C_3H_8$ or $H+C_4H_{10}$ would involve an increase in the number of valence terms in MM energy and the number of van der Waals interactions in the VB/MM energy but would not require new parameters or more expensive quantum-mechanical (semiempirical VB) calculations, although one may have to reoptimize the set of parameters used in defining the switching functions to reproduce the desired geometries and frequencies at the saddle point. The desired values for the exothermicity, barrier height, and shape of the barrier can be achieved by optimizing a small number of parameters in the VB term.

We investigated the effect of anharmonicity by using the HR approximation. The calculated rate constants agree well with experimental results. The KIE for $H+C_2H_6/D+C_2H_6$ shows different temperature dependences in different temperature regions due to the interplay of the contributions from the vibrational partition function and the contributions from tunneling.

Finally, we provide a few remarks to place this work in context. The CVBMM method may be considered to be a special case of the combined quantum-mechanical and molecular mechanical (QM/MM) method, which has been reviewed elsewhere.[117–122] The various combined QM/MM methods are distinguished by the choice of QM treatment and by the way that the QM and MM subsystems are joined together. For example, the QM method may be semiempirical molecular-orbital theory,[123–133] *ab initio* wave-function theory[83,124,134–141] (WFT), or density-functional theory[83,124,142–148] (DFT). Here, following Raff[20] and Joseph *et al.*,[24] we use semiempirical valence bond theory for the QM part. As far as joining the QM and MM parts, the present treatment is very similar to the way QM is joined to MM in previous work.[83,124,136,149] The advantage of CVBMM over previous combined QM/MM methods is that the potential evaluations are very rapid, and one can obtain very precise and inexpensive analytical gradients and Hessians for classical dynamics. The disadvantage is that semiempirical valence bond theory has less predictive value than high-level WFT or DFT. However, this limitation can be overcome by fitting the parameters to higher-level calculations, as is done in the example $H+C_2H_6$ presented in this article.

ACKNOWLEDGMENT

This work was supported in part by the U.S. Department of Energy, Office of Basic Energy Sciences.

[1] D. R. Herschbach, H. S. Johnston, K. S. Pitzer, and R. E. Powell, J. Chem. Phys. **25**, 736 (1956).
[2] H. S. Johnston, Adv. Chem. Phys. **3**, 131 (1960).
[3] S. W. Benson, in *Thermochemical Kinetics*, 2nd ed. (Wiley, New York, 1976).
[4] D. G. Truhlar and B. C. Garrett, J. Am. Chem. Soc. **111**, 1232 (1989).
[5] E. W. R. Steacie and N. W. F. Phillips, J. Chem. Phys. **4**, 461 (1936).
[6] R. Wolfgang, Acc. Chem. Res. **2**, 248 (1969).
[7] W. E. Jones and J. L. Ma, Can. J. Chem. **64**, 2192 (1986).
[8] D. L. Baulch, C. J. Cobos, R. A. Cox *et al.* J. Phys. Chem. Ref. Data **21**, 411 (1992).
[9] V. D. Knyazev, A. Bencsura, S. I. Stoliarov, and I. R. Slagle, J. Phys. Chem. **100**, 11346 (1996).
[10] M. G. Bryukov, I. R. Slagle, and V. D. Knyazev, J. Phys. Chem. A **105**, 3107 (2001).
[11] J. W. Sutherland, M.-C. Su, and J. V. Michael, Int. J. Chem. Kinet. **33**, 669 (2001).
[12] V. D. Knyazev, J. Phys. Chem. A **106**, 11603 (2002).
[13] G. J. Germann, Y.-D. Huh, and J. J. Valentini, J. Chem. Phys. **96**, 5746 (1992).
[14] M. G. Bryukov, I. R. Slagle, and V. D. Knyazev, J. Phys. Chem. A **105**, 6900 (2001).
[15] V. V. Azatyan and S. B. Filippov, Dokl. Phys. Chem. **184**, 49 (1969).
[16] D. Jones, P. A. Morgan, and J. H. Purnell, J. Chem. Soc., Faraday Trans. 1 **73**, 1311 (1977).
[17] J. Lede and J. Villermaux, Can. J. Chem. **56**, 392 (1978).
[18] J. E. Nicholas and G. L. Vaghjiani, J. Chem. Phys. **89**, 3388 (1988).
[19] K. Morokuma and R. E. Davis, J. Am. Chem. Soc. **94**, 1060 (1972).
[20] L. M. Raff, J. Chem. Phys. **60**, 2220 (1974).
[21] G. C. Schatz, S. P. Walch, and A. F. Wagner, J. Chem. Phys. **73**, 4536 (1980).

[22] G. C. Schatz, A. F. Wagner, and J. T. H. Dunning, J. Phys. Chem. **88**, 221 (1984).
[23] D. G. Truhlar, R. Steckler, and M. S. Gordon, Chem. Rev. (Washington, D.C.) **87**, 217 (1987).
[24] T. Joseph, R. Steckler, and D. G. Truhlar, J. Chem. Phys. **87**, 7036 (1987).
[25] K. K. Baldridge, M. S. Gordon, R. Steckler, and D. G. Truhlar, J. Phys. Chem. **93**, 5107 (1989).
[26] G. A. Natanson, B. C. Garrett, T. N. Truong, T. Joseph, and D. G. Truhlar, J. Chem. Phys. **94**, 7875 (1991).
[27] E. Kraka, J. Gauss, and D. Cremer, J. Chem. Phys. **99**, 5306 (1993).
[28] D. Dobbs and D. A. Dixon, J. Phys. Chem. **98**, 5290 (1994).
[29] T. N. Truong and W. Duncan, J. Chem. Phys. **101**, 7408 (1994).
[30] M. J. T. Jordan and R. G. Gilbert, J. Chem. Phys. **102**, 5669 (1995).
[31] T. Takayanagi, J. Chem. Phys. **104**, 2237 (1996).
[32] T. Taketsugu and M. J. Gordon, J. Chem. Phys. **104**, 2834 (1996).
[33] J. Espinosa-Garcia and J. C. Corchado, J. Phys. Chem. **100**, 16561 (1996).
[34] Z. Konkli, E. Kraka, and D. Cremer, J. Phys. Chem. A **101**, 1742 (1997).
[35] T. Takata, T. Taketsugu, K. Hirao, and M. S. Gordon, J. Chem. Phys. **109**, 4281 (1998).
[36] Y. Kurosaki and T. Takayanagi, Chem. Phys. Lett. **299**, 57 (1999).
[37] H.-G. Yu and G. Nyman, J. Chem. Phys. **111**, 3508 (1999).
[38] A. Fernández-Ramos, E. Martínez-Núñez, Z. Smedarchina, and S. A. Vázquez, Chem. Phys. Lett. **341**, 351 (2001).
[39] D. Y. Wang and J. M. Bowman, J. Chem. Phys. **115**, 2055 (2001).
[40] J. Pu, J. C. Corchado, and D. G. Truhlar, J. Chem. Phys. **115**, 6266 (2001).
[41] H.-G. Yu and G. Nyman, J. Phys. Chem. A **105**, 2240 (2001).
[42] B. J. Lynch and D. G. Truhlar, J. Phys. Chem. A **105**, 2936 (2001).
[43] R. Sumathi, H.-H. Carstensen, and J. W. H. Green, J. Phys. Chem. A **105**, 6910 (2001).
[44] G. D. Billing, Chem. Phys. **277**, 325 (2002).
[45] J. Pu and D. G. Truhlar, J. Chem. Phys. **116**, 1468 (2002).
[46] J. Espinosa-Garcia, J. Chem. Phys. **116**, 10664 (2002).
[47] J. Palma, J. Echave, and D. C. Clary, J. Phys. Chem. A **106**, 8256 (2002).
[48] J. Pu and D. G. Truhlar, J. Chem. Phys. **117**, 1479 (2002).
[49] M. L. Wang and J. Z. H. Zhang, J. Chem. Phys. **117**, 3081 (2002).
[50] H. Szichman and R. Baer, J. Chem. Phys. **117**, 7614 (2002).
[51] J. Pu and D. G. Truhlar, J. Chem. Phys. **117**, 10675 (2002).
[52] X. Zhang, G. H. Yang, K. L. Han, M. L. Wang, and J. Z. H. Zhang, J. Chem. Phys. **118**, 9266 (2003).
[53] Y. Zhao, B. J. Lynch, and D. G. Truhlar, J. Phys. Chem. A **108**, 2715 (2004).
[54] Y. Zhao, T. Yamamoto, and W. H. Miller, J. Chem. Phys. **120**, 3100 (2004).
[55] T. Wu, H. J. Werner, and V. Manthe, Science **306**, 2227 (2004).
[56] J. P. Senosiain, C. B. Musgrave, and D. M. Golden, J. Phys. Chem. A **105**, 1669 (2001).
[57] B. C. Garrett and D. G. Truhlar, J. Phys. Chem. **83**, 1079 (1979).
[58] D. G. Truhlar, A. D. Isaacson, and B. C. Garrett, in *Theory of Chemical Reaction Dynamics*, edited by M. Baer (CRC, Boca Raton, FL, 1985), Vol. 4, p. 65.
[59] Y.-P. Liu, G. C. Lynch, T. N. Truong, D.-H. Lu, D. G. Truhlar, and B. C. Garrett, J. Am. Chem. Soc. **115**, 2408 (1993).
[60] B. Kerkeni and D. C. Clary, J. Chem. Phys. **121**, 6809 (2004).
[61] *Combined Quantum Mechanical and Molecular Mechanical Methods*, edited by J. Gao and M. A. Thompson (American Chemical Society, Washington, DC, 1998).
[62] J. Gao and D. G. Truhlar, Annu. Rev. Phys. Chem. **53**, 467 (2002).
[63] N. L. Allinger, J. Am. Chem. Soc. **99**, 8127 (1977).
[64] N. L. Allinger, Y. H. Yuh, and J.-H. Lii, J. Am. Chem. Soc. **111**, 8551 (1989).
[65] J.-H. Lii and N. L. Allinger, J. Am. Chem. Soc. **111**, 8566 (1989).
[66] J.-H. Lii and N. L. Allinger, J. Am. Chem. Soc. **111**, 8576 (1989).
[67] T. C. Allison and D. G. Truhlar, in *Modern Methods for Multidimensional Dynamics Computations in Chemistry*, edited by D. L. Thompson (World Scientific, Singapore, 1998), p. 618.
[68] I. S. Y. Wang and M. Karplus, J. Am. Chem. Soc. **95**, 8160 (1973).
[69] D. J. Malcome-Lawes, J. Chem. Soc., Faraday Trans. 2 **71**, 1183 (1973).
[70] C. Leforestier, J. Chem. Phys. **68**, 4406 (1978).
[71] E. Uggerud and T. Helgakar, J. Am. Chem. Soc. **114**, 4265 (1992).
[72] Y.-Y. Chuang and D. G. Truhlar, J. Chem. Phys. **112**, 1221 (2000).
[73] A. Gonzalez-Lafont, T. N. Truong, and D. G. Truhlar, J. Phys. Chem. **95**, 4618 (1991).
[74] P. Winget, J. D. Thompson, J. D. Xidos, C. J. Cramer, and D. G. Truhlar, J. Phys. Chem. A **106**, 10707 (2002).
[75] C. A. Parr and D. G. Truhlar, J. Phys. Chem. **75**, 1844 (1971).
[76] D. G. Truhlar, R. Steckler, and M. S. Gordon, Chem. Rev. (Washington, D.C.) **87**, 217 (1987).
[77] G. C. Schatz, Rev. Mod. Phys. **61**, 669 (1989).
[78] H. Eyring and G. E. Kimball, J. Chem. Phys. **1**, 239 (1933).
[79] M. B. Faist and J. T. Muckerman, J. Chem. Phys. **71**, 225 (1979).
[80] J. P. Bowen and N. L. Allinger, Rev. Comput. Chem. **2**, 81 (1991).
[81] A. R. Leach, *Molecular Modeling*, 2nd ed. (Prentice-Hall, Harlow, England, 2001).
[82] E. B. Wilson, J. C. Decius, and P. C. Cross, *Molecular Vibrations* (Dover, New York, 1980).
[83] H. Lin and D. G. Truhlar, J. Phys. Chem. A **109**, 3991 (2005).
[84] See EPAPS Document No. E-JCPSA6-123-013544 for a brief description of canonical variational theory, factorization analysis of the KIEs, functional forms of relevant MM3 equations, list of MM3 parameters, rate constants calculated by the TST/W method based on harmonic vibrations and using MPW54/6-31+G(d,p), and the CVBMM potential-energy surface. This document can be reached via a direct link in the online article's HTML reference section or via the EPAPS homepage (http://www.aip.org/pubservs/epaps.html).
[85] B. C. Garrett, D. G. Truhlar, R. S. Grev, and A. W. Magnuson, J. Phys. Chem. **84**, 1730 (1980).
[86] D. G. Truhlar and B. C. Garrett, Annu. Rev. Phys. Chem. **35**, 159 (1984).
[87] S. C. Tucker and D. G. Truhlar, in *New Theoretical Concepts for Understanding Organic Reactions*, edited by J. Bertran and I. G. Csizmadia (Kluwer, Dordrecht, 1989), Vol. 267, p. 291.
[88] B. C. Garrett and D. G. Truhlar, in *Encyclopedia of Computational Chemistry*, edited by P. v. R. Schleyer, N. L. Allinger, T. Clark, J. Gasteiger, P. A. Kollman, H. F. Schaefer III, and P. R. Schreiner (Wiley, Chichester, 1998), Vol. 5, p. 3094.
[89] D.-h. Lu, T. N. Troung, V. S. Melissas, *et al.* Comput. Phys. Commun. **71**, 235 (1992).
[90] D. G. Truhlar, J. Comput. Chem. **12**, 266 (1991).
[91] H. Lin, Y. Zhao, B. A. Ellingson, J. Pu, and D. G. Truhlar, J. Am. Chem. Soc. **127**, 2830 (2005).
[92] L. A. Curtiss, P. C. Redfern, K. Raghavachari, and J. A. Pople, J. Chem. Phys. **114**, 108 (2001).
[93] Y. Zhao, B. J. Lynch, and D. G. Truhlar, Phys. Chem. Chem. Phys. **7**, 43 (2005).
[94] B. J. Lynch and D. G. Truhlar, J. Phys. Chem. A **107**, 3898 (2003).
[95] J. M. L. Martin and G. D. Oliveira, J. Chem. Phys. **111**, 1843 (1999).
[96] J. W. Ochterski, G. A. Petersson, and J. A. Montgomery, Jr., J. Chem. Phys. **104**, 2598 (1996).
[97] B. J. Lynch, P. L. Fast, M. Harris, and D. G. Truhlar, J. Phys. Chem. A **104**, 4811 (2000).
[98] A. D. Becke, J. Chem. Phys. **104**, 1040 (1996).
[99] C. Adamo and V. Barone, J. Comput. Chem. **19**, 419 (1998).
[100] K. Burke, J. P. Perdew, and Y. Wang, in *Electronic Density Functional Theory: Recent Progress and New Directions*, edited by J. F. Dobson, G. Vignale, and M. P. Das (Plenum, New York, 1998), p. 81.
[101] M. J. Frisch, G. W. Trucks, H. B. Schlegel *et al.*, GAUSSIAN 03, revision C.01 (Gaussian, Inc., Pittsburgh, PA, 2003).
[102] B. J. Lynch, Y. Zhao, and D. G. Truhlar, J. Phys. Chem. A **107**, 1384 (2003).
[103] R. Krishnan, J. S. Binkley, R. Seeger, and J. A. Pople, J. Chem. Phys. **72**, 650 (1980).
[104] H.-J. Werner, P. J. Knowles, R. D. Amos *et al.*, MOLPRO, 2002.6 (University of Birmingham, Birmingham, AL, 2002).
[105] Y. Zhao and D. G. Truhlar, MLGAUSS, version 1.0 (University of Minnesota, Minneapolis, MN, 2004).
[106] J. C. Corchado, Y.-Y. Chuang, E. L. Coitiño, and D. G. Truhlar, GAUSSRATE-9.0, 9.0/P9.0-G94/G98 (University of Minnesota, Minneapolis, MN, 2002).
[107] J. C. Corchado, Y.-Y. Chuang, P. L. Fast *et al.*, POLYRATE–9.1 (University of Minnesota, Minneapolis, MN, 2002).
[108] D. G. Truhlar, http://comp.chem.umn.edu/mccdir/software.htm
[109] R. J. Duchovic, Y. L. Volobuev, G. C. Lynch, D. G. Truhlar, T. C. Allison, A. F. Wagner, B. C. Garrett, and J. C. Corchado, Comput. Phys. Commun. **144**, 169 (2002); **156**, 319(E) (2004).
[110] R. J. Duchovic, Y. L. Volobuev, G. C. Lynch, A. W. Jasper, D. G. Truhlar, T. C. Allison, A. F. Wagner, B. C. Garrett, J. Espinosa-García, and J. C.

Corchado, POTLIB online:; http://comp.chem.umn.edu/potlib
[111] M. Page and J. W. McIver, J. Chem. Phys. **88**, 922 (1988).
[112] Y. Zhao, B. J. Lynch, and D. G. Truhlar, J. Phys. Chem. A **108**, 4786 (2004).
[113] K. A. Nguyen, C. F. Jackels, and D. G. Truhlar, J. Chem. Phys. **104**, 6491 (1996).
[114] J. M. Rodgers, P. L. Fast, and D. G. Truhlar, J. Chem. Phys. **112**, 3141 (2000).
[115] A. D. Bosese and J. M. L. Martin, J. Chem. Phys. **121**, 3405 (2004).
[116] B. Kerkeni and D. C. Clary, J. Chem. Phys. **120**, 2308 (2004).
[117] J. Gao, Rev. Comput. Chem. **7**, 119 (1996).
[118] P. Sherwood, in *Modern Methods and Algorithms of Quantum Chemistry*, edited by J. Grotenhaus (Neumann Institute for Computing, Jülich, 2000), p. 285.
[119] J. Gao and D. G. Truhlar, Annu. Rev. Phys. Chem. **53**, 467 (2002).
[120] A. Shurki and A. Warshel, Adv. Protein Chem. **66**, 249 (2003).
[121] R. A. Friesner and V. Guallar, Annu. Rev. Phys. Chem. **56**, 389 (2005).
[122] H. Lin and D. G. Truhlar, Theor. Chem. Acc. (to be published).
[123] M. J. Field, P. A. Bash, and M. Karplus, J. Comput. Chem. **11**, 700 (1990).
[124] P. D. Lyne, M. Hodoscek, and M. Karplus, J. Phys. Chem. A **103**, 3462 (1999).
[125] J. J. Ruiz-Pernia, E. Silla, I. Tunon, S. Marti, and V. Moliner, J. Phys. Chem. B **108**, 8427 (2004).
[126] J. Pu, J. Gao, and D. G. Truhlar, J. Phys. Chem. A **108**, 5454 (2004).
[127] M. P. Gleeson, I. H. Hillier, and N. A. Burton, Org. Biomol. Chem. **2**, 2275 (2004).
[128] H. Park, E. N. Brothers, and K. M. Merz, Jr., J. Am. Chem. Soc. **127**, 4232 (2004).
[129] P. L. Cummins and J. E. Gready, J. Comput. Chem. **26**, 561 (2005).
[130] B. A. Gregersen, J. Khandogin, W. Thiel, and D. M. York, J. Phys. Chem. B **109**, 9810 (2005).
[131] S. Ferrer, J. J. Ruiz-Pernia, I. Tuñon, V. Moliner, M. Garcia-Viloca, A. Gonzalez-Lafont, and J. M. Lluch, J. Chem. Theory Comput. **1**, 750 (2005).
[132] O. Acevedo and W. L. Jorgensen, J. Am. Chem. Soc. **127**, 8829 (2005).
[133] H. Hu and W. Yang, J. Chem. Phys. **123**, 41102 (2005).
[134] M. Freindorf and J. Gao, J. Comput. Chem. **17**, 386 (1996).
[135] X. Assfeld and J.-L. Rivail, Chem. Phys. Lett. **263**, 100 (1996).
[136] J. Pu, J. Gao, and D. G. Truhlar, J. Phys. Chem. A **108**, 632 (2004).
[137] D. Xu, H. Guo, J. Gao, and Q. Cui, Chem. Commun. (Cambridge) **7**, 892 (2004).
[138] A. Osted, J. Kongsted, K. V. Mikkelsen, and O. Christiansen, J. Phys. Chem. A **108**, 8646 (2004).
[139] J. H. Jensen, H. Li, A. D. Robertson, and P. A. Molina, J. Phys. Chem. A **109**, 6634 (2005).
[140] M. Klaehn, S. Braun-Sand, E. Rosta, and A. Warshel, J. Phys. Chem. B **109**, 15645 (2005).
[141] Q. M. Fatmi, T. S. Hofer, B. R. Randolf, and B. M. Rode, J. Chem. Phys. **123**, 054514 (2005).
[142] I. Tuñon, M. T. C. Martins-Costa, C. Millot, and M. F. Ruiz-Lopez, J. Chem. Phys. **106**, 3633 (1997).
[143] P. M. Dal, L. I. Llarrull, U. Rothlisberger, A. J. Vila, and P. Carloni, J. Am. Chem. Soc. **126**, 12661 (2004).
[144] J.-W. Chu, B. R. Brooks, and B. L. Trout, J. Am. Chem. Soc. **126**, 16601 (2004).
[145] M. Hoffmann, I. V. Khavrutskii, D. G. Musaev, and K. Morokuma, Int. J. Quantum Chem. **99**, 972 (2004).
[146] A. A. Sokol, S. T. Bromley, S. A. French, C. Catlow, A. Richard, and P. Sherwood, Int. J. Quantum Chem. **99**, 695 (2004).
[147] G. Drudis-Sole, G. Ujaque, F. Maseras, and A. Lledos, Chem.-Eur. J. **11**, 1017 (2005).
[148] H. M. Senn, D. O'Hagan, and W. Thiel, J. Am. Chem. Soc. **127**, 13643 (2005).
[149] J. Pu, J. Gao, and D. G. Truhlar, ChemPhysChem **6**, 1853 (2005).